The International Journal of Advanced Manufacturing Technology (2024) 132:5683–5694
https://doi.org/10.1007/s00170-024-13708-3

ORIGINAL ARTICLE

Strengthening and precipitation hardening mechanisms of surface-mechanically treated 17-4PH stainless steel

Temitope Olumide Olugbade[1,2] · Bankole I. Oladapo[1,2] · Qi Zhao[1] · Tin Tin Ting[2]

Received: 2 February 2024 / Accepted: 27 April 2024 / Published online: 6 May 2024

Abstract
Achieving ultra-high strength without sacrificing too much ductility is the focus of attention in nanostructured materials. Here, the strengthening mechanism and property enhancement of surface-mechanically treated 17-4PH stainless steel (SS17-4PH) were investigated. Our findings show that a grain refinement and elongated lath-like martensitic grain (~ 50 nm thick) could be produced after surface treatment. The grain size remains in the nanoscale, and random crystallographic orientations with the presence of nanocrystallites characterize the nanocrystalline grains formed on the treated sample. This contributes to the property enhancement with a yield strength of about 901 MPa and a reduced elongation to failure of about 17%. The atom probe tomography (APT) characterization unveiled the emergence of high-density precipitate (Cu-rich) at the material surface, with a number density of about 2.6255×10^{24} m^{-3} and an average radius of 2.22 nm. Besides, the dislocation activities caused by SMAT result in the gradual breakdown of precipitates into smaller sizes and final dissolution in the matrix, increasing the number of nucleation sites and leading to more grain refinement processes. The grain boundary, dislocation densities, and the Cu-rich precipitate greatly influence the strengthening mechanism of surface-treated SS17-4PH.

Keywords Strengthening mechanism · Sustainable manufacturing · SS17-4PH · Process innovation · Precipitates

1 Introduction

Improving the hardness and strength of metallic materials is one of the long-term dreams of many materials experts. This has been actualized with time via the surface nanocrystallization technique, which helps prepare gradient-structured layers on sample surface with improved surface properties (1–2). Nanostructured materials are receiving massive attention due to their remarkable properties, such as high hardness, better fatigue properties, and improved ductility without sacrificing ultrahigh strength [1–4].

As a form of martensitic precipitation hardened steel, compared to other steels, SS17-4PH is an important material with several industrial applications ranging from high-strength shafts, jet engine parts, gears, chemical process equipment, valves, and nuclear reactor components (3–4). Many automotive and aerospace industries prefer using SS17-4PH among the family of steels due to its remarkable properties, including moderate corrosion resistance, high strength and hardness for enhanced reliability, good toughness, and ease of fabrication [5, 6]. However, SS17-4PH still experiences failure, especially under fluctuating stress, aggressive corrosive environment, and high-cycle fatigue. Most of these failures initiate at the surface and propagate to the core region before the final breakdown. Hence, there is a need for proper surface treatment to protect the material surface further. Some of the surface treatment techniques adopted in the past to enhance the metallic materials' mechanical properties by refining the grains to ultra-fined grained include ultrasonic peening, cold rolling, extrusion, depositions, and surface mechanical attrition treatment (SMAT) [7–14].

Compared to other nanocrystallization processes, SMAT is well known for generating a gradient-structured material with improved properties without altering the inherent properties [15–18]. In this method, a plastic deformation produces an ultrafine grain on the treated material. In the past, the unique SMAT technique has been

✉ Temitope Olumide Olugbade
tolugbade001@dundee.ac.uk

[1] School of Science and Engineering, University of Dundee, Dundee, UK

[2] Faculty of Data Science and Information Technology, INTI International University, Persiaran Perdana BBN, Putra Nilai, Malaysia

Table 1 Chemical composition of the as-received SS17-4PH sample and the concentrations measured by APT (at%), together with the atomic error obtained after three rounds of experiments

Element	C	Mn	Si	Cr	Ni	Co	V	Cu	Nb	Fe
Bulk	0.070	1.000	1.000	15.500	4.500	0.060	0.050	3.500	0.300	74.020
APT	0.370	0.315	0.850	17.305	4.920	0.019	0.032	3.255	0.055	72.879
Error (±)	0.005	0.005	0.009	0.029	0.020	0.002	0.003	0.016	0.002	0.034

successfully applied to different metallic materials, including carbon steels [19], iron [20, 21], aluminum [22, 23], titanium [24, 25], and steel [26, 27]. Until now, the effect of surface processing by a novel SMAT technique on the microstructures, mechanical properties, and the anti-wear performance of SS17-4PH has not been fully investigated. More importantly, the strengthening and precipitation hardening mechanism of SS17-4PH after surface treatment by SMAT remains unclear.

In the present study, we investigated the outstanding strengthening and precipitation hardening mechanism in surface-mechanically treated (SMATed) SS17-4PH by carefully studying the influence of grain boundary and dislocation densities caused by SMAT leading to a raise in nucleation sites numbers, as well as the Cu-rich precipitates located at the material surface. The gradient-structured formed on the SMAT-processed SS17-4PH sample characterized by random crystallographic orientations with the presence of nanocrystallites, together with the high-density Cu-precipitates, could be related to the strengthening mechanism with a high yield strength (~ 901 MPa), bending strength (~ 1820 MPa), and a lower wear volume which is about one-third that of the as-received counterpart.

2 Experimental

2.1 Sample preparation and SMAT process

A commercial SS17-4PH steel ($100 \times 100 \times 4$ mm^3) was selected in this study. The compositions of the as-received sample and the concentrations measured by atom probe tomography (APT) (at%) are summarized in Table 1. After cutting the samples into sizes, they were degreased with acetone before the SMAT treatment. The sample was treated on both surfaces for 20 min in this study with free-moving multidirectional tungsten carbide (WC) balls. The SMAT procedures have been previously described in detail [9, 28].

2.2 Mechanical and tribology properties

To study the influence of plastic deformation induced by SMAT on the hardness of SS17-4PH steel sample and the extent of surface nanocrystallization, a variation in microhardness across the depth from the treated surface was investigated using Vickers Micro-Hardness Tester with 300 mN load and dwell time of 20 s. To measure the bending strength of the samples with and without SMAT treatment, three-point bending (3 PB) SS17-4PH samples (33 mm x 4 mm x 3 mm) were produced and examined on MTS (USA) 30 kN electro-mechanical material tester, according to ASTM E290-14 standard. An average microhardness and bending strength value were determined after three repeated measurements. The tensile test was carried out on a material tester (extensometer: MTS 632.24 F-50) with a 1.5 mm/min tensile speed. The yield, ultimate tensile strength, as well as the fracture elongation of the samples, were obtained from the stress-strain curve.

The wear tests were performed by a wear tester (TEER ST-3001) using Ø4 mm WC balls, with sliding velocity of 1.5 mm/min, stroke length of 3 mm, and sliding duration of 900 s, under different loads ranging from 2 to 10 N. After the wear test, the profiles of the wear tracks for the as-received and SMATed SS17-4PH samples were immediately analyzed using surface profilometer (Veeco/Wyko NT9300). The software on the profilometer analyzed the wear volume obtained based on the wear tracks.

The microstructures of the SS17-4PH samples before and after surface treatment by SMAT, as well as the micrographs of the worn surface after wear test, were obtained by scanning electron microscope (SEM-FEI Quanta 450 FEG) with an operating voltage of 20 kV.

2.3 TEM characterization

TEM investigated the grain refinement and the strengthening mechanism of the SMAT-processed SS17-4PH. The TEM sample was prepared via a focused ion beam (FIB), AURIGA-Germany. The TEM observations were conducted on JEOL 2100 F (FE-TEM), operating at 200 kV voltage. At room temperature, the surface compressive residual stress of untreated and SMATed SS17-4PH samples was measured by X-ray stress analyzer (model: XL-640, China) using Cr K_α radiation, with an x-ray tube current of 6 mA and voltage of 26 kV. The residual stress was measured by the standard XRD $\sin^2\psi$ method, with

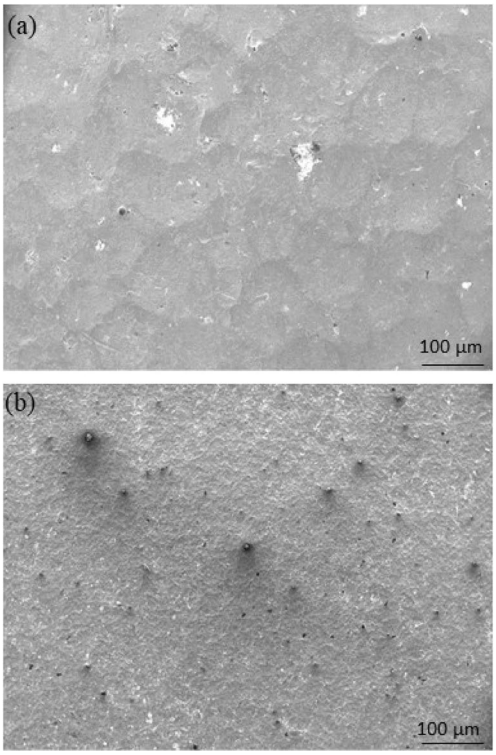

Fig. 1 The SEM microstructures of the SS17-4PH samples before and after surface treatment at room temperature, **a** untreated, **b** treated

an X-ray irradiated area of 2 mm^2, $sin^2\psi$ range of 0–0.5, x-ray elastic constant of 180.0 ± 0.7, diffraction angle of 82.5°, and (211) diffraction plane.

2.4 APT characterization

An advanced APT characterization was carried out to study further the elemental mapping and concentrations across the matrix-surface region. After fabricating the needle-like sample for the APT experiment via the FIB technique, the APT experiment was carried out in voltage mode, with a sample temperature of 70 K, 200 kHz pulses at an evaporation detection rate of 0.3% atom/pulse, and a pulse fraction of 0.2. Using IVAS software, the 3D reconstructions and data analysis were carried out to assess the structure and composition of all elements.

3 Results

3.1 Microstructure evolution

During SMAT operation, the collision of the WC spherical hardened balls on the surface of the SS17-4PH sample causes plastic deformation and compressive residual stress during the treatment. The SEM microstructures of the SS17-4PH samples before and after surface treatment are shown in Fig. 1. The surface-mechanically treated SS17-4PH samples are characterized with many deformations, surface defects, and high surface roughness (Fig. 1b) compared to the untreated one (Fig. 1a) which reveals grain size and sample microstructure without surface treatment. The deformations are often produced after surface treatment, and the extent of deformation largely depends on treatment time and ball size [26]. A 25–35 µm grain size was obtained for the untreated sample. In contrast, SMAT operation led to nanostructure surface layers with reduced grain size. This induces surface roughness and compressive residual stress, improving the hardness and overall strength of SS17-4PH. However, more strain-induced martensitic layers were generated on the sample surface after treatment.

TEM observation was carried out to better understand the mechanism and nanostructure, which induced high hardness and strength in SS17-4PH compared to other stainless steels. As evident in the cross-sectional TEM images (Fig. 2), lamella nanocrystallites (Fig. 2a) and dislocations (Fig. 2b) were formed.

The formation of the nanocrystallites may result from high strains with a high strain rate-induced treatment. This results in a significant improvement in hardness and strength compared to other steels. As shown in Fig. 2c, lath martensite and dislocation clusters exist in the submicron-sized section of SS17-4PH. According to the cross-sectional TEM images (Fig. 2d1, d3) and the corresponding SAED pattern (Fig. 2d2, d4), longitudinal lath-like martensitic grains are identified in the sample after SMAT treatment, with lath boundary represented by a red dashed line. Strengthening from martensite comes from a few factors, such as dislocation density and the lath thickness [28]. The smaller the lath thickness, the better the strength and hardness. The surface grains refinement of SMATed SS17-4PH was characterized by the formation of mechanical twinning [1], followed by the formation of randomly oriented nanocrystallites.

The TEM micrographs with dark field (DF) and bright field (BF) views are shown in Fig. 3a and b, with information on the microstructures of the SS17-4PH sample after SMAT. As shown in Fig. 3c, the diffraction pattern shows the diffraction spots arranged in circles. SMAT reduces the grain size at the surface layer. However, the grain size increases gradually from the upper layer to the matrix [29]. The TEM profile shows that the grain size of the treated sample remains in the nanoscale (Fig. 3e). The nanocrystalline grains formed on the SMATed sample are characterized by lamella structure (Fig. 3d) and random crystallographic orientations [30], with a nanoscale grain refinement and the generation of an elongated lath-like martensitic grains (~ 50 nm thick). This supports the formation of nano-martensite during SMAT.

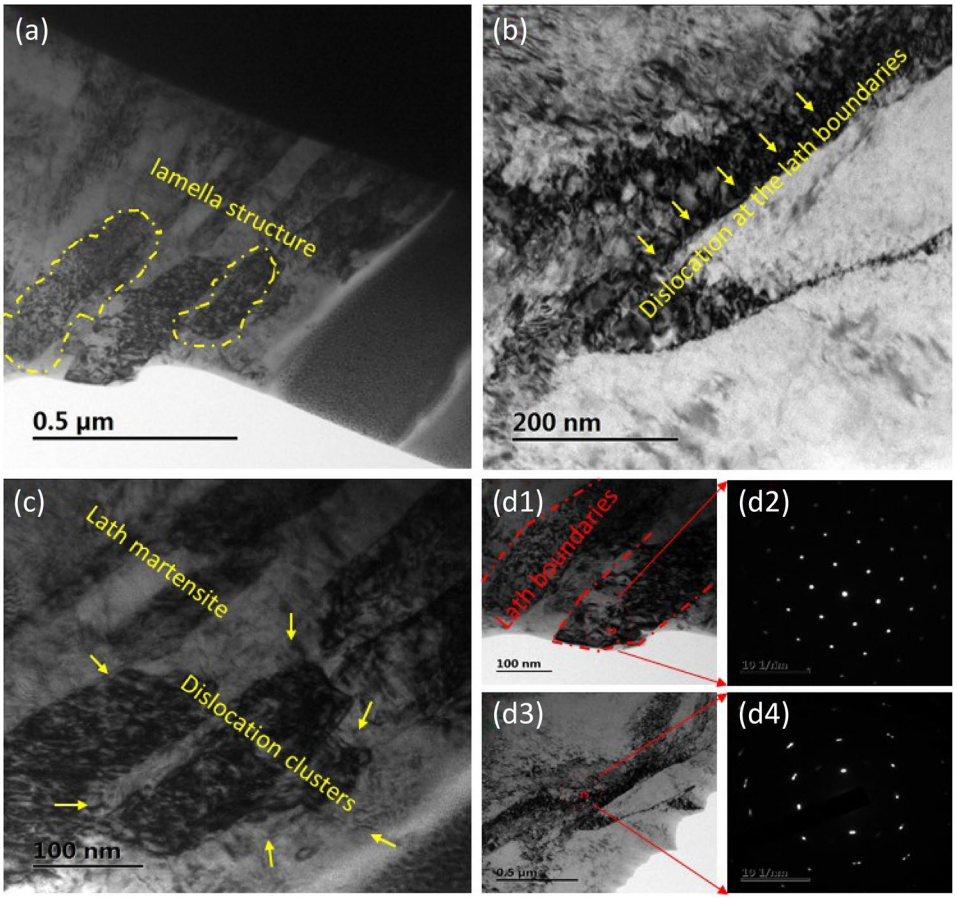

Fig. 2 Cross-sectional TEM images in the top surface layer of SS17-4PH showing the **a** lamellar structures, **b** dislocation at the lath boundaries as a result of the effects of SMAT treatment, **c** lath martensite and dislocation clusters in the sub-micro-sized section, **d1** and **d3** typical martensitic laths in the sample after treatment, lath boundary is represented by red dashed line, **d2** shows the corresponding SAED pattern in the region taken from the circle in **d1**, **d4** shows the corresponding SAED pattern in the region taken from the circle in **d3**

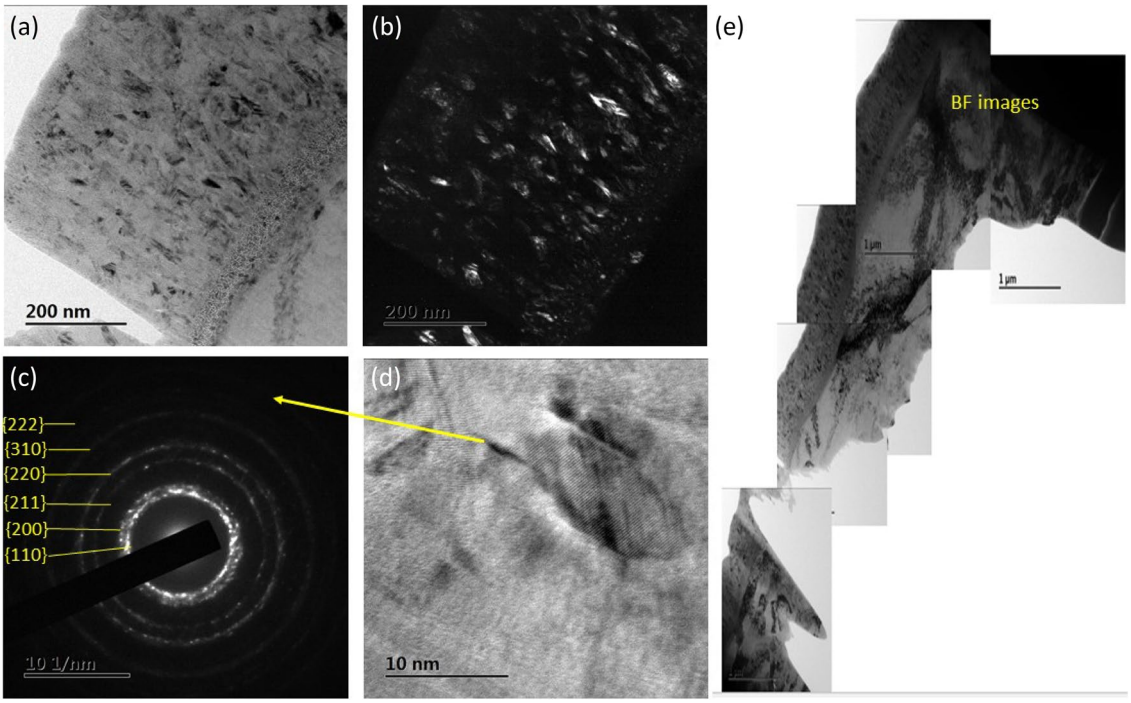

Fig. 3 **a** Bright-field and **b** dark-field TEM images (in the reflex 110-Fe) showing microstructures of the surface layer in the SMAT treated SS17-4PH sample, **c** corresponding selected area electron diffraction (SAED) patterns of **d** with [222], [310], [220], [211], [200], and [110] zone axes **d** lamella structure, **e** BF images with different dislocation

The generation of ultra-fine strain-induced martensitic layers increases the hardness of SS17-4PH compared to the other steels. In addition, the formation of randomly oriented lamella structure (Fig. 3d) and lath martensite phase (mostly BCC) [3], as well as the presence of surface compressive residual stress, could be responsible for the enhanced micro-hardness exhibited by the treated SS17-4PH sample. The high hardness and strength can also be linked to the lath thickness of the martensite.

3.2 Mechanical properties

The surface roughness increases after SMAT with an average roughness of 4.55 µm, unlike the as-received sample with roughness of 2.18 µm. This change in roughness can be ascribed to the formation of dimples and spots [31] after the impingement of the SMAT shots on the SS17-4PH sample surface. In addition, treatment time and ball size are the major factors influencing surface roughness [19]. The influence of surface roughness on materials after treatment was also emphasized in the literature [32, 33]. Figure 4a shows the variations of micro-hardness across depth for SS17-4PH samples before and after treatment. The hardness of the treated sample increases after SMAT. As indicated in Fig. 4a, the hardness of all samples decreased gradually from the upper layer to the base layer of the material. The SMATed sample exhibited a higher hardness value of 453 HV in the top surface nanostructured layer. The insert represents the surface hardness with and without SMAT treatment. With the surface hardness value of about 285 HV for the sample before SMAT and 503 HV for the treated sample, it is also confirmed that SMAT can significantly enhance the surface microhardness and the hardness across depth. Figure 4b shows the three-point bending strength of all SS17-4PH samples. The untreated SS17-4PH was found to have a bending strength value of 810 MPa. In contrast, after treatment, the SMATed sample exhibited a higher bending strength value of 1820 MPa.

The enhancement in the microhardness and bending strength of SS17-4PH could result from the high density of dislocations [3] in a nano-surface layer and the strain-hardening effect [1]. Besides, the surface compressive residual stress induced before and after SMAT was measured to know the extent of deformation after treatment. The as-received SS17-4PH sample possessed a compressive residual stress of 120 MPa. Meanwhile, the SMATed sample experienced a more compressive residual stress of 415 MPa. The surface compressive residual stress induced by SMAT helps prevent the initiation and propagation of cracks [34, 35] on the material surface. It thus enhances the material's fatigue life, stiffness, and overall strength.

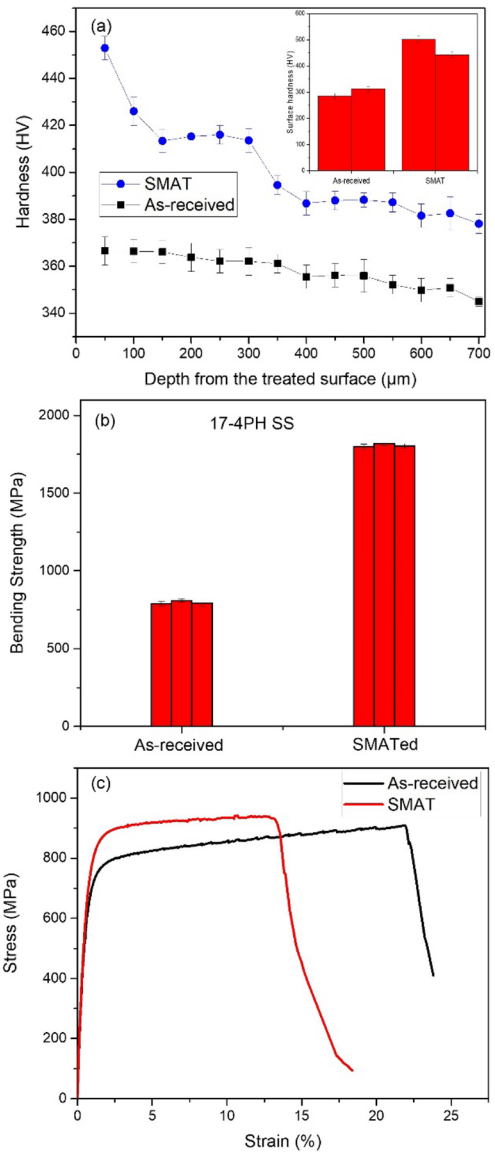

Fig. 4 Mechanical properties after surface treatment by SMAT using Ø3 mm WC balls for 20 min; **a** micro-hardness distribution of the as-received and SMATed SS17-4PH samples along the depth from the treated surface (The insert represents the surface microhardness of the samples with 300 mN load and dwell time of 20 s), **b** bending strength of the as-received and SMATed SS17-4PH samples, **c** tensile engineering stress–strain curve for the as-received and treated SS17-4PH samples

By SMAT, the yield strength of the SS17-4PH sample could be improved from 795 to 901 MPa, with a reduced elongation to failure of about 17%. (Fig. 4c). The improvement in yield strength experienced by the SMAT sample can be attributed to the high compressive residual stress induced during treatment, grain refinement and work-hardening effect [1, 3, 9] because of the plastic deformation resulting from the bombardment of the sample surface with the repeated multidirectional high-velocity

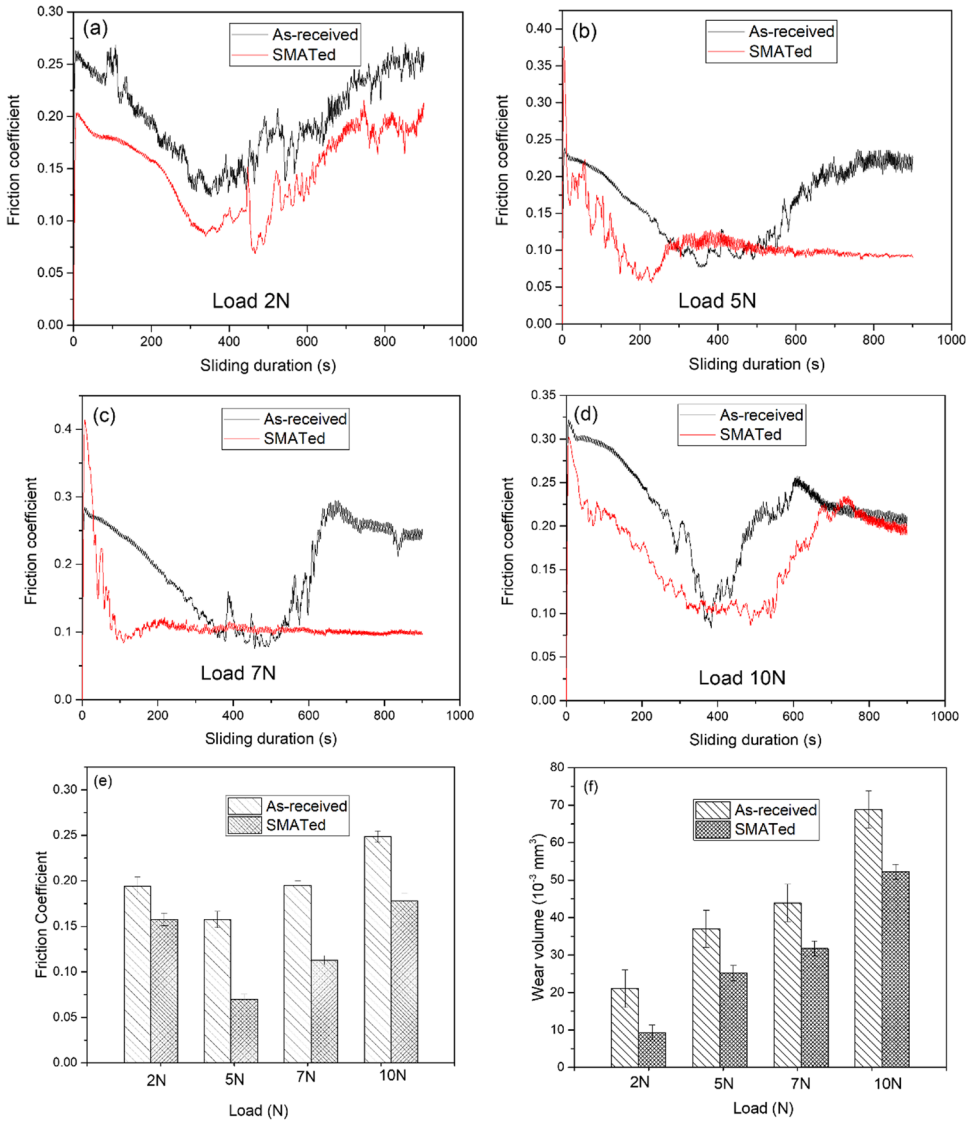

Fig. 5 Friction coefficient evolution during the wear test of SS17-4PH using Ø4 mm WC balls, sliding velocity of 1.5 mm/min, stroke length of 3 mm, and sliding duration of 900 s, under different loads of **a** 2 N, **b** 5 N, **c** 7 N, and **d** 10 N; **e** corresponding average friction coefficient between the as-received and SMATed SS17-4PH samples; **f** variation of wear volume with the applied load of 2 N, 5 N, 7 N, and 10 N for the as-received and SMATed SS17-4PH samples

moving balls. In addition, the grain refinement effect may be ascribed to the activity of the high dislocation density experienced during the SMAT treatment.

3.3 Tribological properties

The friction coefficient evolution during the wear test as a function of sliding duration using Ø4 mm WC balls under different loads of 2 N, 5 N, 7 N, and 10 N is shown in Fig. 5a–d. Under a testing load of 2 N (Fig. 5a), the friction coefficient for the SS17-4PH samples before and after SMAT shows similar tendencies. The SMATed SS17-4PH sample exhibits a lower friction coefficient than the sample before treatment. As a function of load, the corresponding average friction coefficient for the SS17-4PH samples before and after treatment is shown in Fig. 5e. The treated SS17-4PH sample exhibited lower friction coefficients and enhanced wear resistance under all the testing loads from 2 N to 10 N due to the grain refinement induced by the SMAT process. For example, under the load of 5 N, the as-received sample possesses an average friction coefficient of 0.1577. In contrast, the SMATed sample exhibited a smaller friction coefficient, which means that SMAT is a good technique for improving the anti-wear performance of materials.

The variation of wear volume with the applied load for SS17-4PH steels with and without treatment is illustrated in Fig. 5f. For both samples, the wear volume increases with increasing applied load. Under all the testing loads, the wear volume of the SMATed SS17-4PH sample is lower than that of the as-received sample, especially under low load conditions where the wear volume was observed to be one-third that of the as-received sample under 2 N. This implies that wear volume is a function of the applied load, and surface

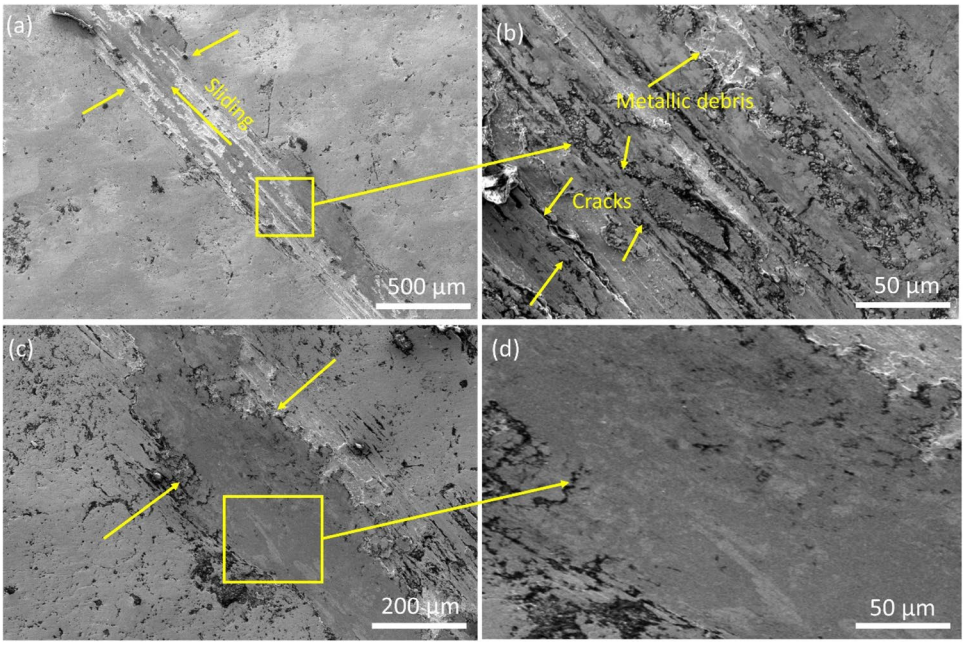

Fig. 6 SEM micrographs of the worn surface of SS17-4PH after wear test using Ø4 mm WC ball, sliding velocity of 1.5 mm/min, sliding distance of 3 mm, and sliding duration of 900 s, under load 10 N: **a** as-received sample, the opposite arrows indicate the wear track; **b** enlarged A, denoted by the square box in **a**, with the presence of metallic debris and cracks, as a result of wear; **c** SMATed sample, the opposite arrows indicate the wear track; **d** enlarged C, denoted by the square box in **c**

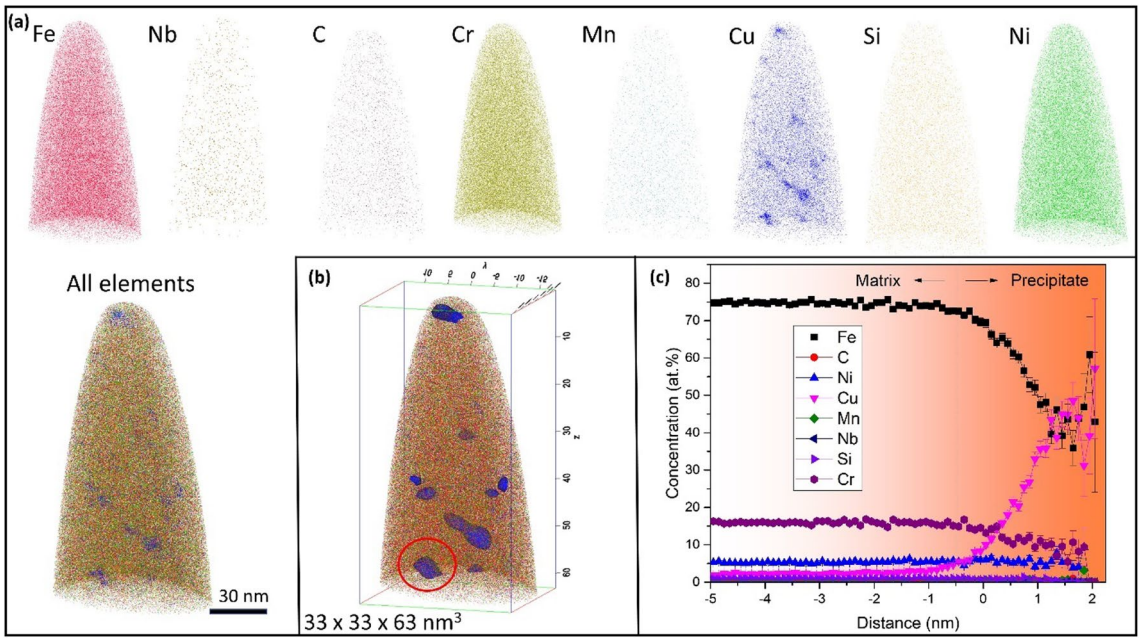

Fig. 7 APT characterization of the SS17-4PH sample after surface treatment by SMAT at room temperature. **a** Atom maps of Fe, Ni, C, Cr, Mn, Cu, and Si elements (all denotes "all elements"). **b** APT map displaying the atomic-scale distribution of all elements, with reconstruction volume of $33 \times 33 \times 63$ nm^3 and containing millions of ions (the red circle denotes the presence of Cu precipitate). **c** Proximity histogram constructed across the interfaces between the matrix and precipitates

treatment by SMAT can enhance the wear resistance of the SS17-4PH sample.

Figure 6 represents the SEM images of the worn surface of SS17-4PH after the wear test using Ø4 mm WC ball with a sliding distance of 3 mm under load 10 N. As indicated in Fig. 6a and b, metallic debris and cracks are present in the as-received SS17-4PH sample due to the wear action. Meanwhile, the effect of the wear process is less on the SMATed sample (Fig. 6c and d), hence an improved anti-wear property. This further demonstrates the strength and ability of the SMAT process to improve the surface properties of metallic materials.

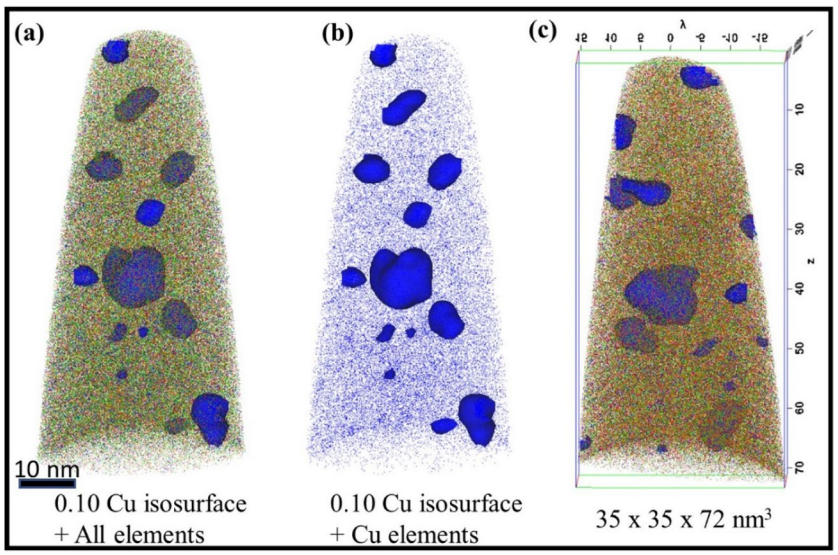

Fig. 8 Elements concentration for the SMAT-processed SS17-4PH sample; **a** 0.10 Cu isosurface + all elements, **b** 0.10 Cu isosurface + Cu elements, and **c** APT map displaying the atomic-scale distribution of all elements, with reconstruction volume of $35 \times 35 \times 72$ nm^3 and containing millions of ions

3.4 Precipitate evolution and dissolution

The SMAT process significantly influences the elemental distribution from the matrix region to the surface region. APT technique assessed and characterized the atomic-scale distribution of all elements and their concentrations with the distance from the surface. Figure 7 shows the APT characterization of the SS17-4PH sample after surface treatment by SMAT at room temperature. The elemental mapping of Fe, Nb, Ni, C, Cr, Mn, Cu, and Si elements is revealed in Fig. 7a. The APT map in Fig. 7b displays the high-resolution atomic-scale distribution of all elements, with a reconstruction volume of $33 \times 33 \times 63$ nm^3 containing millions of ions.

The presence of Cu precipitate (denoted by the red circle in Fig. 7b) is noticeable, as confirmed in Fig. 8, with the elemental composition of 0.1 at% Cu concentration isosurface. The Cu-alloy precipitates are delineated with an isoconcentration level of 0.1 at% to ensure individual separation of the precipitates from the matrix. The proximity histogram in Fig. 7c, showing the variations of concentration of all elements with the distance from the surface, was constructed across the interfaces between the matrix and precipitates based on 0.1 at% Cu concentration isosurface. The presence of Nb element was more obvious for the SMAT-processed SS17-4PH sample, as shown in the atom maps (Fig. 7a and b). Figure 8 shows the iso-concentration of Cu precipitate for the 0.10 Cu isosurface with all elements (Fig. 8a) and with Cu elements only (Fig. 8b), and the atomic-scale distribution of all elements (Fig. 8c) with Cu as the main precipitate, for the SMAT-processed SS17-4PH sample. The Fe and Cr elements fall in the matrix interface, while the Cu element dominates in the precipitate interface. In contrast, Ni, Si, Mn, and C neither belong to the matrix nor precipitate interface.

4 Discussion

4.1 Influence of SMAT on microstructures and properties

In the present study, SMAT changed the microstructural orientation with grain refinement from the base to the top layer and caused a plastic deformation, which significantly enhanced the anti-wear performance and mechanical properties of SS17-4PH, including the bending strength, surface compressive residual stress, and microhardness (Figs. 1, 2, 3, 4, 5, and 6). The microstructural refinement may be linked to the high-density of copper precipitates in the sample. The enhanced mechanical properties suggest that SMAT could refine the microstructure of a material to a nanoscale and induce surface compressive residual stress on the treated sample, which is high enough to prevent crack initiation and formation [34] and other defects that may affect the properties of materials. Due to the high strain stored and repeated loading during SMAT treatment, a similar change in microstructure and improvement in mechanical properties was also achieved during the plastic deformation of nanocrystalline-grained tungsten prepared by SMAT [3]. The results suggest that SMAT could significantly enhance metallic materials' hardness, overall strength, and ductility [1, 2]. The mechanical properties (surface compressive residual stress and hardness) were also improved during the plastic deformation of SS17-4PH using the shot peening technique [36, 37]. In addition, the mechanical properties further increased when the shot-peened SS17-4PH process was subjected to additional heat treatment [38]. In line with the microstructural and the surface compressive residual stress analysis, the overall improvement of strength and

Table 2 The average chemical compositions obtained from APT data for the SS17-4PH across the matrix and precipitate interfaces based on 0.1 at% Cu concentration isosurface

Sample		Composition (at%)						
		Fe	Ni	C	Cr	Mn	Cu	Si
SS17-4PH	Matrix	74.73 ± 0.45	5.44 ± 0.98	0.50 ± 0.36	16.30 ± 0.38	0.32 ± 0.06	1.92 ± 0.14	0.94 ± 0.09
	Precipitate	35.92 ± 4.73	4.11 ± 2.32	0.48 ± 0.47	9.38 ± 5.15	0.68 ± 0.67	57.14 ± 18.70	0.41 ± 0.40

hardness of SMATed SS17-4PH may be linked to the effect of microstructure refinement, dislocation density improvement as well as the compressive residual stress because of the multidirectional impact loading as well as the high strain rate induced during SMAT process.

4.2 Elements distribution and precipitation details

SMAT could not only strengthen the SS17-4PH steel with enhanced microstructure, mechanical, and tribological properties but also contribute to the redistribution of elements, as shown in Fig. 7. The APT analysis unveiled the emergence of precipitate (Cu-rich) at the material surface. This may be due to the large density of Cu observed in the sample compared with other elements [39, 40]. In addition, it seems the element samples are not randomly distributed. From the elements' atomic-scale distribution (Fig. 7b), elemental segregation in the volume was observed. This further confirms the uneven distribution of all elements. The presence of either Cu or Ni plays a vital role in refining the grains. In contrast, combining both elements significantly strengthens the SS17-4PH sample through grain refinement.

Although Ni did not form an individual precipitate, Cu-containing material in the presence of Ni significantly raises the number density of precipitates, thereby improving the grain refinement process and improving strength. The fact that the presence or addition of Ni significantly promotes Cu nucleation and nanoprecipitation is in good agreement with the previous results [41–44]. Besides, compared to the effect of Mn, the addition of Ni greatly enhanced the number density of Cu precipitates, reducing the critical energy for nucleation when compared with Mn [42, 43]. Osamura et al. [44]. also confirm the precipitation of Cu by adding Ni, leading to improved properties.

The number density (D) of the precipitates within the reconstruction, estimated to be 2.6255×10^{24} m^{-3}, was determined using the following relationship:

$$D = \frac{a\eta}{NQ}$$

Herein, η represents the detection efficiency of the atom probe, N denotes the total number of atoms in the reconstruction, Q is the volume of one solute atom, and a represents the number of volume clusters.

4.3 Strengthening mechanism

As a result of treatment by SMAT, the grain-refinement mechanism in SS17-4PH involves the formation of dense dislocation walls in original grains and the transformation of dislocations into sub-boundaries with small misorientation (Figs. 2 and 3). This is perfectly in line with the Hall-Petch relationship, which has been recognized in the past by various researchers as the major strengthening mechanism behind the surface treatment by SMAT [9, 45–48]. As the high-velocity moving balls continuously hit the material surface, high dislocation density occurs, generating ultrafine/nanocrystalline grain size [49–52] and influencing the surface properties [53, 54].

In addition, SMAT causes dislocation activities, ultimately influencing the degree of precipitation and grain refinement process, hence a change in element distributions [39, 42]. In the present study, high density precipitates (Cu-rich) in the 17-4PH steel sample were noticed after surface treatment by SMAT. With the number density value of 2.6255×10^{24} m^{-3} and an average radius of 2.22 nm, the presence of the precipitate, which is rightly located at the sample surface, may positively influence the properties of SS17-4PH. In addition, the presence of Nb element is more pronounced for the SMAT-processed SS17-4PH sample than the as-received sample. Nb is a unique alloying element for strength [46], and its presence may further strengthen the sample with improved properties. The precipitates may also contribute to the strengthening mechanism in SS17-4PH. It is believed that the hardening treatment will influence the subsequent aging of the steel, and this is expected due to the resulting redistribution of components in the defective layer.

Considering the proximity histogram in Fig. 7c, the Fe and Cr elements fall in the matrix interface while the Cu element was dominant in the precipitate interface. However, neither C, Mn, Si, and Ni belong to the precipitate nor matrix interface. The chemical compositions of the elements in both matrix and precipitate interfaces obtained from APT data are summarized in Table 2, with Fe and Cu taking the largest values of 74.73 ± 0.45 and 57.14 ± 18.70 at% on matrix and precipitate sides, respectively.

The concentration peaks of C, Mn, and Si tend to be lower than 2%, whereas the concentration peak of Ni can be as high as 4%. The concentration peak of Ni surpasses that

of C, Si, and Mn, indicating that Ni segregates more than C, Si, and Mn. However, the concentration of Fe tends to increase to a certain point and then monotonically decreases. The enrichment of Cu change also follows the monotonic manner with an increase towards the interface side. Out of the saturated matrix, about 36% of Cu was precipitated as revealed in the analysis for the atomic ratios of Cu in matrix and precipitate interfaces.

To sum it up, the overall strengthening mechanism of SMAT-processed SS17-4PH is related to the grain boundary, dislocation densities, and activities caused by SMAT, which results in the gradual breakdown of precipitates into smaller sizes and final dissolution in the matrix, hence an increase in the number of nucleation sites, leading to more grain refinement process.

5 Conclusion

In summary, the strengthening, property enhancement, and precipitation hardening mechanisms of surface mechanically treated SS17-4PH were investigated by TEM, SEM-EDS, and 3D-APT. The following points were deduced.

(1) TEM characterization formed a grain refinement and elongated lath-like martensitic grain (~ 50 nm thick) on the gradient-structured material. It was found that the grain size of the treated sample remains in the nanoscale, and random crystallographic orientations characterize the nanocrystalline grains formed on the treated sample. In addition, a high volume of nano-lath martensite structures and phases exists with the presence of nanocrystallites and many substructures with interfaces, which supports the formation of nano-martensite during treatment. The grain-refinement mechanism involves the formation of dense dislocation walls in original grains and transforming dislocations into sub-boundaries with small misorientation.

(2) The mechanical and tribological properties were significantly enhanced with a yield strength of about 901 MPa, and elongation to failure was reduced by about 17%. The bending strength and microhardness could be as high as 1820 MPa and 453 HV, respectively. In addition, a lower wear volume of about one-third that of the as-received counterpart can be achieved for the SMAT-processed sample due to the grain refinement effect, indicating that surface treatment by SMAT can significantly enhance the wear resistance.

(3) The microstructural changes observed and improved mechanical properties and anti-wear performance of SS17-4PH can be attributed to the multidirectional impact loading leading to the density of dislocations and the high strain rate induced during the SMAT process.

(4) The APT analysis unveiled the emergence of precipitate (Cu-rich) at the material surface, with a density of about $2.6255 \times 1024\ m-^{3}$ and an average radius of 2.22 nm. This means that the elements in the sample are not randomly distributed. The APT map displays the high-resolution atomic-scale distribution of all elements, with a reconstruction volume of $33 \times 33 \times 63\ nm^{3}$ containing millions of ions. In addition, the presence of Nb element was more evident for the SMAT-processed sample when compared with the as-received counterpart. It is believed that the high-density Cu-rich precipitates at the material surface and the presence of Nb element obtained after SMAT may contribute to the strengthening mechanism.

Acknowledgements T.O. Olugbade acknowledges Prof. J. Lu and the Centre for Advanced Structural Materials (CASM) for the SMAT technique. The efforts of Dr. J. Liu and Dr. J. Luan are highly acknowledged and appreciated for their assistance in the TEM and APT experiments, respectively.

Data availability The raw/processed data required to reproduce these findings cannot be shared at this time as the data also forms part of an ongoing study.

Declarations

Competing interests The authors declare no competing interests.

References

1. Guo H, Xia M, Chan L, Wang K, Zhang X, Yan Q, He M, Lu J, Ge C (2017) Nanostructured laminar tungsten alloy with improved ductility by surface mechanical attrition treatment. Sci Rep 7:1351
2. Kou H, Lu J, Li Y (2016) High-strength and high-ductility nanostructured and amorphous metallic materials. Adv Mater 26:5518–5524
3. Guo H, Xia M, Wu Z, Chan L, Dai Y, Wang K, Yan Q, He M, Ge C, Lu J (2017) Nanocrystalline-grained tungsten prepared by surface mechanical attrition treatment: microstructure and mechanical properties. J Nucl Mater 480:281–288

4. Olugbade TO, Olutomilola EO, Olorunfemi BJ (2022) Review of passivity and electrochemical properties of nanostructured stainless steels obtained by surface mechanical attrition treatment (SMAT): trend and progress. Corros Rev 40:189–203
5. Sowa R, Kowal A, Roga E, Arabasz S, Dziedzic A, Dul I, Parlinska-Wojtan M (2015) Influence of double solution treatment on hardness in 17–4 PH steel. Zastita Materijala 56:261–268
6. Olugbade TO (2022) Passivation behaviour of surface-treated 17-4PH stainless steel in chloride-containing environment with varying concentrations. Chem Afr 5:333–340
7. Olugbade TO, Omiyale BO, Ojo OT, Adeyeri MK (2023) Stress-corrosion and corrosion-fatigue properties of Surface-treated Aluminium Alloys for Structural Applications. Chem Afr 6:1699–1708
8. Olugbade TO, Omoniyi OO, Omiyale BO (2022) Electrochemical properties of heat-treated Al alloy A6061-T6 in 0.5 M H_2SO_4 solution. J Inst Eng India Ser D 103:141–147
9. Lu K, Lu J (2004) Nanostructured surface layer on metallic materials induced by surface mechanical attrition treatment. Mater Sci Eng A 375–377:38–45
10. Olugbade TO, Abioye TE, Farayibi PK, Olaiya NG, Omiyale BO, Ogedengbe TI (2020) Electrochemical properties of MgZnCa-based thin film metallic glasses fabricated by magnetron sputtering deposition coated on a stainless steel substrate. Anal Lett 54:1588–1602
11. Ying L, Wu G, Liu L, Lu J (2019) A new inner surface attrition treatment for strengthening metallic tubular structures. Adv Eng Mater 21:1801125
12. Lee HS, Kim DS, Jung JS, Pyoun YS, Shin K (2009) Influence of peening on the corrosion properties of AISI 304 stainless steel. Corros Sci 51:2826–2830
13. Mohammed T, Olugbade TO, Nwankwo I (2016) Determination of the effect of oil exploration on galvanized steel in Niger Delta. Nigeria J Sci Res Rep 10:1–9
14. Wang T, Yu J, Dong B (2006) Surface nanocrystallization induced by shot peening and its effect on corrosion resistance of 1Cr18Ni9Ti stainless steel. Surf Coat Technol 200:4777–4781
15. Lu K, Lu J (2004) Nanostructured surface layer on metallic materials induced by surface mechanical attrition treatment. Mater Sci Eng A 375:38–45
16. Koch CC (2003) Top-down synthesis of nanostructured materials: mechanical and thermal processing methods. Rev Adv Mater Sci 5:91–99
17. Wu G, Chan K, Zhu L, Sun L, Lu J (2017) Dual-phase nanostructuring as a route to high-strength magnesium alloys. Nature 545:80–83
18. Liu G, Lu J, Lu K (2000) Surface nanocrystallization of 316L stainless steel induced by ultrasonic shot peening. Mater Sci Eng A 286:91–95
19. Balusamy T, Sankara Narayanan TSN, Ravichandran K (2012) Effect of surface mechanical attrition treatment (SMAT) on boronizing of EN8 steel. Surf Coat Technol 213:221–228
20. Tao NR, Wang ZB, Tong WP, Sui ML, Lu J, Lu K (2002) An investigation of surface nanocrystallization mechanism in. Fe induced by surface mechanical attrition treatment. Acta Mater 50:4603–4616
21. Wang ZB, Tao NB, Li S, Wang W, Liu G, Lu J, Lu K (2003) Effect of surface nanocrystallization on friction and wear properties in low carbon steel. Mater Sci Eng A 352:144–149
22. Wu X, Tao N, Hong Y, Lu J, Lu K (2005) Localized solid-state amorphization at grain boundaries in a Nanocrystalline Al solid solution subjected to surface mechanical attrition. J Phys D: Appl Phys 38:4140–4143
23. Chang HW, Kelly PM, Shi YN, Zhang MX (2012) Thermal stability of nanocrystallized surface produced by surface mechanical attrition treatment in aluminum alloys. Surf Coat Technol 206:3970–3980
24. Zhang L, Han Y (2010) Effect of nanostructured titanium on anodization growth of self- organized TiO_2 nanotubes. Nanotechnology 21:055602
25. Zhu KY, Vassel A, Brisset F, Lu K, Lu J (2004) Nanostructure formation mechanism of α-titanium using SMAT. Acta Mater 52:4101–4110
26. Chen AY, Ruan HH, Wang J, Chan HL, Wang Q, Li Q, Lu J (2011) Optimization of the strain rate to achieve exceptional mechanical properties of 304 stainless steel using high speed ultrasonic surface mechanical attrition treatment. Acta Mater 59:3697–3709
27. Laleh M, Kargar F (2011) Suppression of chromium depletion and sensitization in austenitic stainless steel by surface mechanical attrition treatment. Mater Lett 65:1935–1937
28. Lu K, Lu J (1999) Surface nanocrystallization (SNC) of metallic materials-presentation of the concept behind a new approach. J Mater Sci Technol 15:193–197
29. Zhang HW, Hei ZK, Liu G, Lu J, Lu K (2003) Formation of nanostructured surface layer on AISI 304 stainless steel by means of surface mechanical attrition treatment. Acta Mater 51:1871–1881
30. Lin Y, Lu J, Wang L, Xu T, Xue Q (2006) Surface nanocrystallization by surface mechanical attrition treatment and its effect on structure and properties of plasma nitrided AISI 321 stainless steel. Acta Mater 54:5599–5605
31. Balusamy T, Kumar S, Sankara Narayanan TSN (2010) Effect of surface nanocrystallization on the corrosion behavior of AISI 409 stainless steel. Corros Sci 52:3826–3834
32. Kumar CS, Urbikain G, Fernandes F, Rjoub AAL, De López LN (2024) Influence of V concentration in TiAlSiVN coating on self-lubrication, friction and tool wear during two-pass dry turning of austenitic steel 316 L. Tribol Int 193:109355
33. Arifvianto B, Suyitno M, Mahardika P, Dewo PT, Iswanto UA, Salim (2011) Effect of surface mechanical attrition treatments (SMAT) on microhardness, surface roughness, and wettability of AISI 316L. Mater Chem Phys 125:418–426
34. Ya M, Xing Y, Dai F, Lu K, Lu J (2003) Study of residual stress in surface nanostructured AISI 316L stainless steel using two mechanical methods. Surf Coat Technol 168:148–155
35. Olugbade TO (2023) Review: corrosion resistance performance of severely plastic deformed aluminium based alloys via different processing routes. Met Mater Int 29:2415–2443
36. AlMangour B, Yang J (2016) Improving the surface quality and mechanical properties by shot-peening of 17–4 stainless steel fabricated by additive manufacturing. Mater Des 110:914–924
37. Karthik D, Kalainathan S, Swaroop S (2015) Surface modification of 17–4 PH stainless steel by laser peening without protective coating process. Surf Coat Technol 278:138–145
38. AlMangour B, Yang J (2017) Integration of heat treatment with shot peening of 17–4 stainless steel fabricated by direct metal laser sintering. JOM 69:2309–2313
39. Jiao ZB, Luan JH, Zhang ZW, Miller MK, Ma WB, Liu CT (2013) Synergistic effects of Cu and Ni on Nanoscale precipitation and mechanical properties of high-strength steels. Acta Mater 61:5996–6005
40. Kong HJ, Xu C, Bu CC, Da C, Luan JH, Jiao ZB, Chen G, Liu CT (2019) Hardening mechanisms and impact toughening of a high-strength steel containing low ni and Cu additions. Acta Mater 172:150–160
41. Olugbade TO (2020) Stress corrosion cracking and precipitation strengthening mechanism in TWIP steels: progress and prospects. Corros Rev 38:473–488
42. Zhang C, Enomoto M (2006) Study of the influence of alloying elements on Cu precipitation in steel by non-classical nucleation theory. Acta Mater 54:4183–4191

43. Seko A, Nishitani SR, Tanaka I, Eiichi HA, Fujita F (2004) First-principles calculation on free energy of precipitate nucleation. Calphad 28:173–176
44. Osamura K, Okuda H, Asano K, Furusaka M, Kishida K, Kurosawa F, Uemori R (1994) SANS study of phase decomposition in Fe-Cu alloy with Ni and Mn addition. ISIJ International 34(1994):346–354
45. Roland T, Retraint D, Lu K, Lu J J (2006) Fatigue life improvement through surface nanostructuring of stainless steel by means of surface mechanical attrition treatment. Scr Mater 54:1949–1954
46. Jóni B, Schafler E, Zehetbauer M, Tichy G, Ungár T (2013) Correlation between the microstructure studied by X-ray line profile analysis and the strength of high-pressure-torsion processed Nb and Ta. Acta Mater 61:632–642
47. Olugbade TO (2022) Passive film analysis and corrosion study of steel type 301 after mechanical deformation. MRS Adv 7:886–891
48. Olugbade TO, Omiyale BO (2022) Corrosion study and surface analysis of the passivation film on surface-deformed AISI 304 stainless steel. Chem Afr 5:1663–1670
49. Zhu Y, Huang J, Gubicza J, Ungár T, Wang Y, Ma E, Valiev R (2003) Nanostructures in Ti processed by severe plastic deformation. J Mater Res 18:1908–1917
50. Olugbade TO, Ojo OT, Omiyale BO, Olutomilola EO, Olorunfemi BJ (2021) A review on the corrosion fatigue strength of surface-modified stainless steels. J Brazilian Soc Mech Sci Eng 43:421
51. Gubicza J, Chinh N, Krállics G, Schiller I, Ungar T (2006) Microstructure of ultrafine-grained FCC metals produced by severe plastic deformation. Curr Appl Phys 6:194–199
52. Olugbade TO (2021) Electrochemical characterization of the corrosion of mild steel in saline following mechanical deformation. Anal Lett 54:1055–1067
53. López de Lacalle LN, Rodríguez A, Lamikiz A, Celaya A, Alberdi R (2011) Five-Axis Machining and Burnishing of Complex Parts for the improvement of Surface Roughness. Mater Manuf Processes 26:997–1003
54. Rodriguez A, de Lacalle LNL, Pereira O et al (2020) Isotropic finishing of austempered iron casting cylindrical parts by roller burnishing. Int J Adv Manuf Technol 110:753–761